

Predictive torque and flux control for the synchronous reluctance machine

R. MORALES* and M. PACAS

Institute of Power Electronics and Electrical Drives (LEA), University of Siegen, D-57068 Siegen, Germany

Abstract. This paper presents a predictive torque and flux control algorithm for the synchronous reluctance machine. The algorithm performs a voltage space phasor pre-selection, followed by the computation of the switching instants for the optimum switching space phasors, with the advantages of inherently constant switching frequency and time equidistant implementation on a DSP based system. The criteria used to choose the appropriate voltage space phasor depend on the state of the machine and the deviations of torque and flux at the end of the cycle.

The model of the machine has been developed on a d-q frame of coordinates attached to the rotor and takes into account the magnetic saturation in both d-q axes and the cross saturation phenomenon between both axes. Therefore, a very good approximation of this effect is achieved and the performance of the machine is improved.

Several simulations and experimental results using a DSP and a commercially available machine show the validity of the proposed control scheme.

Key words: predictive torque control, flux prediction, synchronous reluctance machine, magnetic cross saturation.

1. Introduction

After new improvements in rotor design the synchronous reluctance machine (SyncRel) today is a viable alternative to induction machines, to permanent magnet excited synchronous machines and to switched reluctance machines in low-power drive applications [1–9]. The main points in favor of this choice are the low cost and the easier field weakening capability. It has theoretically no rotor losses and depending on the saliency, it has a torque density comparable with the induction machine.

On the other hand, the complexity of the dynamic equations of the SyncRel is increased due to the different magnetic characteristics in the direct and quadrature (d-q) axes. It is very well known that the saturation of both inductances L_d and L_q not only depends on the current in the same axis but also on the current in the orthogonal axis [2,3]. As a result, the control of SyncRel faces some special problems different to the other AC machines.

Direct self (DSC) and direct torque controls (DTC) that were first developed for the induction machines [10,11], have been used also on the SyncRel, since they show an excellent dynamic performance, DSC and DTC have been continuously improved and have experimented a further evolution.

In [5] a quasi-analogue implementation of the conventional DTC for the SyncRel was described. In order to reduce torque and current pulsations, a DTC-SVM scheme and Torque Vector Control (TVC) variants have also been proposed for the SyncRel [6–9] a kind of sensorless (DSC) control was presented.

The conventional DTC that selects the active voltage space phasor and the zero voltage space phasor by using a switching table [11] has merits of simple structure and easy implemen-

tation, whereas it shows some drawbacks such as switching frequency variation and a high sampling frequency needed for the digital implementation.

To solve these problems, a Direct Mean Torque Control (DMTC) and later an improved algorithm of DMTC for the induction machine were proposed [12–14]. DMTC is a kind of DTC, which calculates the “on” time of the switches in a way that steady state value of the torque is directly reached at the end of the cycle.

This type of Predictive Torque Control (PTC) and its digital implementation were also proved for the permanent magnet synchronous machine [15], where an excellent torque dynamic with PTC has been demonstrated.

This paper presents an appropriate algorithm for digital implementation of the Predictive Torque Control proposed in [13] for the SyncRel. Simulations and experimental results using a DSP and a commercially available machine show the validity of the proposed control scheme.

2. Improved direct mean torque control

Figure 1 shows a typical operation cycle of the improved DMTC [13,14] in steady-state. The switching instants are directly placed in a way that the mean torque over the cycle is equal to the reference value. Applying an active voltage space phasor (AVSP) first, the torque increases at the beginning of the switching interval. In the following, the torque produced by an active voltage space phasor will be designated as M_{AVSP} . Then when the limit of a calculated “virtual hysteresis width (ΔM)” is reached, a zero voltage space phasor (ZVSP) is applied and the torque decreases. The torque produced by a zero voltage space phasor is called M_{ZVSP} .

*e-mail: moralescaporal@uni-siegen.de

In steady-state, the torque $M_{(k)}$ at the beginning of a cycle should be equal to its value $M_{(k+1)}$ at the end (which results in a theoretical zero torque error at the end of a cycle). Instead of simply equalizing the different hatched areas (Fig. 1) for the cycle k , it is also possible to switch the AVSP to reach directly the value of $M_{(k+1)}$ according to steady-state, thus:

$$M_{(k+1)} = M^* - 1/2\Delta M \quad (1)$$

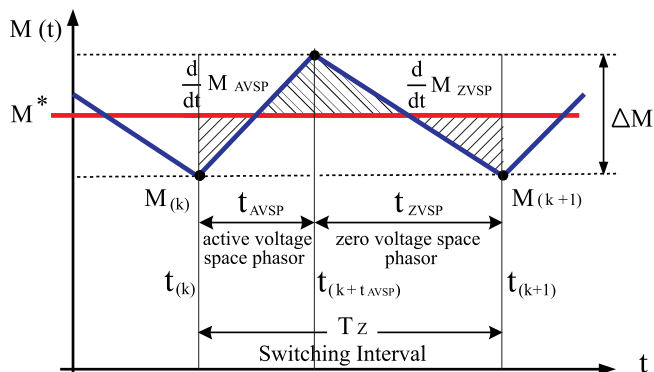


Fig. 1. Typical operation cycle of DMTC in steady-state

The torque $M_{(k+1)}$ at the end of the cycle can be expressed as:

$$M_{(k+1)} = M_{(k)} + \frac{d}{dt}M_{AVSP} \cdot t_{AVSP} + \frac{d}{dt}M_{ZVSP} \cdot (T_Z - t_{AVSP}) \quad (2)$$

By assuming a linear shape of the torque during a switching interval T_Z , in which an AVSP is applied during the time t_{AVSP} and a ZVSP during t_{ZVSP} , the “virtual hysteresis width” in the steady state can be calculated as:

$$\Delta M = - \frac{\frac{d}{dt}M_{AVSP} \cdot \frac{d}{dt}M_{ZVSP}}{\frac{d}{dt}M_{AVSP} - \frac{d}{dt}M_{ZVSP}} \cdot T_Z \quad (3)$$

Solving equation (2) for t_{AVSP} leads finally to:

$$t_{AVSP} = \frac{M^* - M_{(k)} - 1/2 \cdot \Delta M - \frac{d}{dt}M_{ZVSP}T_Z}{\frac{d}{dt}M_{AVSP} - \frac{d}{dt}M_{ZVSP}} \quad (4)$$

and

$$t_{ZVSP} = T_Z - t_{AVSP} \quad (5)$$

The six possible active voltage space phasors have different influences on the torque as well as on the flux. Therefore, sector comparators pre-select the two most favourable voltage space phasors and the “on” time t_{AVSP} is calculated for them.

In each instant, the torque is proportional to the stator flux magnitude, and to the sine of the angle ϑ (see Eq. 8 and Fig. 2).

For constant stator flux, it is clear that a fast torque change can be achieved with a change of the “torque angle” ϑ .

By assuming that the stator flux space phasor $\underline{\Psi}$ is situated in the m -th sector ($m = 1, \dots, 6$) of the α - β plane (Fig. 3); the active voltage spaces phasors $\underline{u}_m, \underline{u}_{m+1}, \underline{u}_{m-1}$ can be selected in order to increase its magnitude. Conversely, its magnitude decreases by applying \underline{u}_{m+2} or \underline{u}_{m-2} .

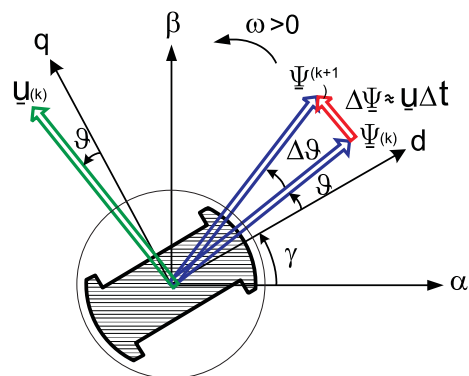


Fig. 2. Variation of motor torque angle according to the selected voltage space phasor

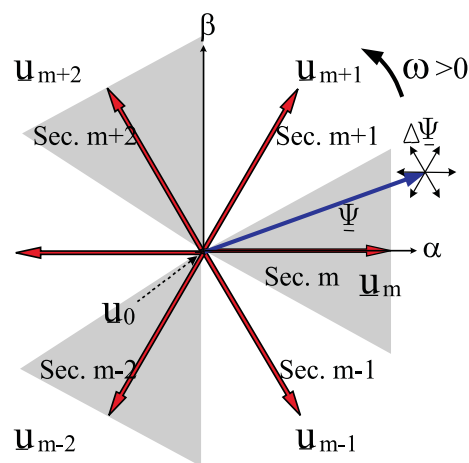


Fig. 3. Voltage space phasors, sectors and stator flux variation

Table 1 summarizes the combined action of each space phasor on both stator flux and torque, for positive rotation ($\omega > 0$).

Table 1
Selection of voltage space phasor ($\omega > 0$)

Voltage space phasor	\underline{u}_{m-2}	\underline{u}_{m-1}	\underline{u}_m	\underline{u}_{m+1}	\underline{u}_{m+2}	\underline{u}_0
Flux	↓	↑	↑↑	↑	↓	↓↑
Torque	↓	↓	↑↓	↑	↑	↓

As it appears evident, for positive speed, an increment of the torque is obtained by selecting two active voltage space phasors only. These are \underline{u}_{m+1} or \underline{u}_{m+2} . The zero voltage space phasor \underline{u}_0 acts on the torque in accordance to the speed direction and does not affect substantially the stator flux.

3. Proposed algorithm for predictive torque and flux control

3.1. Model of the machine. The model of the SyncRel has been developed on a d-q frame of coordinates attached to the rotor and takes into account the magnetic saturation and the

cross magnetic saturation. Thus the SyncRel can be described by the following voltage equations in the rotor reference frame.

$$\begin{aligned} u_d &= R_S i_d + \frac{d}{dt} \Psi_d - \omega \Psi_q, & \Psi_d &= L_d(i_d, i_q) \cdot i_d \\ u_q &= R_S i_q + \frac{d}{dt} \Psi_q + \omega \Psi_d, & \Psi_q &= L_q(i_d, i_q) \cdot i_q \end{aligned} \quad (6)$$

where i_d and i_q are the stator currents in d, q coordinates. R_s denotes the stator resistance, ω is the shaft speed and $L_d(i_d, i_q)$ and $L_q(i_d, i_q)$ denote that the inductances are functions of the both stator currents i_d and i_q .

The electromagnetic torque M is given by:

$$M = \frac{3}{2} p (L_d(i_d, i_q) - L_q(i_d, i_q)) \cdot i_d \cdot i_q \quad (7)$$

where p is the number of pole pairs.

An equivalent expression for the torque can be obtained by using the amplitude of the stator flux and its angle with respect to the d axis.

$$M = \frac{3}{4} p \left(\frac{L_d(i_d, i_q) - L_q(i_d, i_q)}{L_d(i_d, i_q) \cdot L_q(i_d, i_q)} \right) \cdot |\Psi^2| \cdot \sin(2\vartheta). \quad (8)$$

The measurement of the parameters for the SyncRel that is used in the experimental setup and the measurement methods were described in previous works [2–4]. The results of the stationary inductances are shown in Fig. 4, where the cross magnetic saturation phenomenon is very evident.

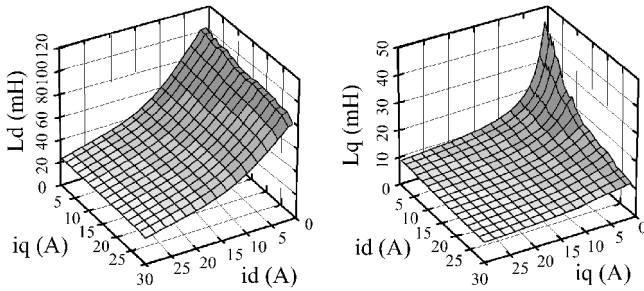


Fig. 4. Measured stationary inductances L_d and L_q

An important task is to reduce the size of the data fields without detriment in the accuracy of the model of the SyncRel. This is especially important for the implementation on a DSP based system. The inductance characteristic is implemented by using polynomials with order 6 ($L_d(i_d)$) and 9 ($L_q(i_q)$) and with linear dependence $L_d(i_q)$ and $L_q(i_d)$.

The cross magnetic saturation has a high impact on the dynamic behavior of the drive and has to be taken into consideration otherwise the prediction becomes inaccurate as it is shown in a different paper [16].

3.2. Torque control. By differentiating (7) and considering that the variation of $L_d(i_d, i_q)$ and $L_q(i_d, i_q)$, in a sufficient small control sampling time are insignificant, then $\frac{d}{dt} M$ can be determined by

$$\frac{d}{dt} M = \frac{3}{2} p (L_d - L_q) \cdot \left(i_d \cdot \frac{d}{dt} i_q + i_q \cdot \frac{d}{dt} i_d \right) \quad (9)$$

where L_d denotes $L_d(i_d, i_q)$ and L_q denotes $L_q(i_d, i_q)$.

By using (6) and (9) and assuming that a ZVSP is applied to the machine the torque decreases and its time derivative is:

$$\begin{aligned} \frac{d}{dt} M_{ZVSP} &= \frac{3}{2} p (L_d - L_q) \\ &\cdot \left\{ \left(\frac{\omega L_q i_q - R_S i_d}{L_d} \cdot i_q \right) - \left(\frac{\omega L_d i_d + R_S i_q}{L_q} \cdot i_d \right) \right\}. \end{aligned} \quad (10)$$

And for an AVSP, the torque increases with the time derivative

$$\begin{aligned} \frac{d}{dt} M_{AVSP} &= \frac{3}{2} p (L_d - L_q) \\ &\cdot \left\{ \left(\frac{u_q i_d}{L_q} \right) + \left(\frac{u_d i_q}{L_d} \right) \right\} + \frac{d}{dt} M_{ZVSP}. \end{aligned} \quad (11)$$

In order to decide which voltage space phasor has to be applied to the machine a second criterion is necessary and the flux has to be taken into account.

3.3. Flux control. The flux control of the conventional DTC method has some problems such as the tracking of the flux trajectory, especially in the low speed region. This phenomenon appears just after the position of the stator flux space phasor moves from one sector into the next sector. The application of the zero voltage space phasor makes it difficult to increase the developed torque when the sector changes.

This problem was handled by a complex flux control algorithm in [13] and an improved flux control for DMTC was presented in [17]. This improvement used a third voltage space phasor for the voltage modulation if it was necessary.

A new method using flux prediction at the end of the switching interval was presented as an alternative solution on the permanent magnet synchronous machine [15]. This strategy is applied in this work to the SyncRel.

The main goal of the flux prediction is to know its magnitude in the next cycle to choose the optimum active voltage space phasor that offers less flux deviation at the end of its “on” time and to keep the stator flux as close as possible on a circular trajectory.

The d and q components of the stator current space phasor can be predicted at the end of the switching interval from the voltage Eq. (6) as:

$$\begin{aligned} i_d(kT + t_{AVSP}) &= \frac{t_{AVSP}}{L_d} \\ &\times \{ u_d(kT) + \omega L_q i_q(k) - R_S i_d(k) \} + i_d(k) \\ i_q(kT + t_{AVSP}) &= \frac{t_{AVSP}}{L_q} \\ &\times \{ u_q(kT) - \omega L_d i_d(kT) - R_S i_q(kT) \} + i_q(kT). \end{aligned} \quad (12)$$

In the same manner, the components of the flux space phasor at the end of the same cycle can be predicted by

$$\begin{aligned} \Psi_d(k + t_{AVSP}) &= L_d i_d(k + t_{AVSP}) \\ \Psi_q(k + t_{AVSP}) &= L_q i_q(k + t_{AVSP}). \end{aligned} \quad (13)$$

Following this strategy the value of the flux and torque ripple are calculated at the beginning of each sampling interval by applying the algorithm developed above for all the possible stator space phasors. Based on the results of the prediction, the control chooses the voltage space phasor and the correspond-

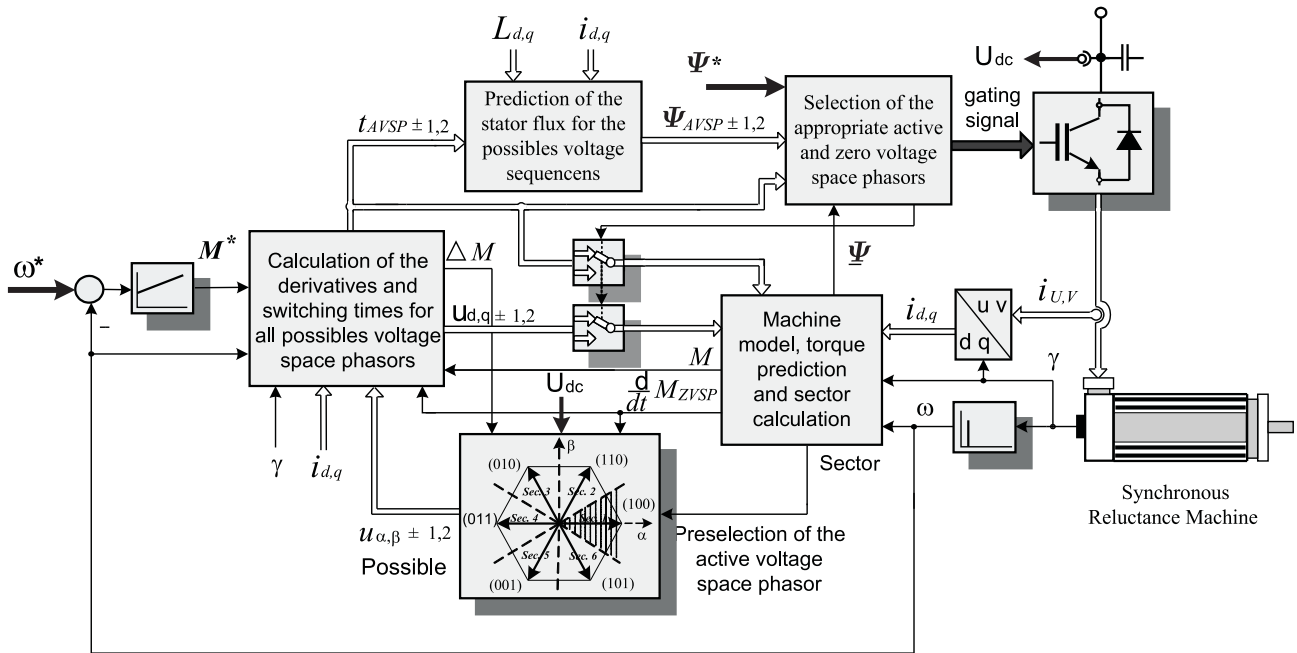


Fig. 5. Control block diagram of the proposed predictive torque control for the synchronous reluctance machine*

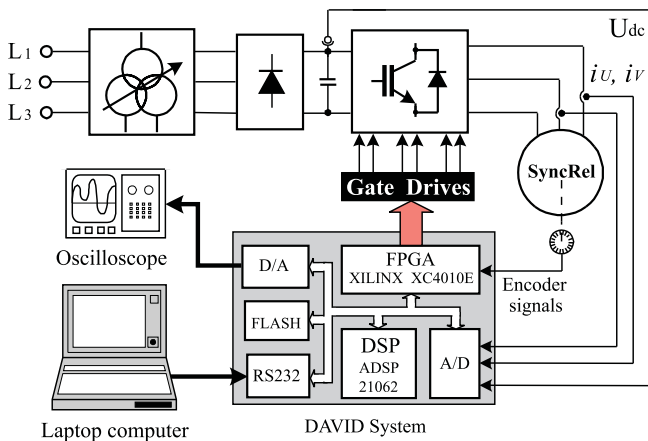


Fig. 6. Configuration of the experimental system

the operating point but it can be calculated in advance and the switching frequency can be kept constant.

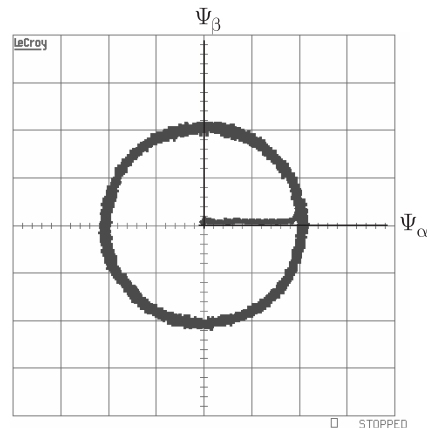


Fig. 8. Experimental stator flux trajectory at start-up (0.2 Vs/div)

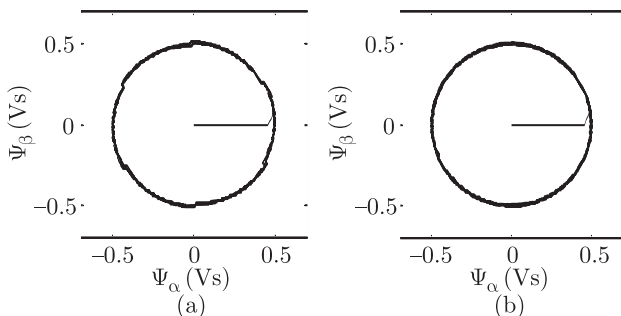


Fig. 7. Simulation of the stator flux trajectory (a) without and (b) with flux prediction algorithm

ing switching time that lead to the best trajectory of the stator flux space phasor. Of course, the torque ripple depends on

4. Simulation and experimental results

In order to verify the behavior of the drive, the predictive torque control scheme developed in this work (Fig. 5) was simulated using Matlab/SIMULINK, and was digitally implemented, by using a dedicated hardware as shown in Fig. 6, consisting of a floating point DSP of Analog Devices (ADSP 21062) and Xilinx-FPGA (XC4010E) device to implement the voltage selection and the encoder signal counter.

The program runs at $T_z = 100 \mu s$, which is also common in field orientated schemes and much longer than in conventional DTC. For the speed feedback, an encoder of 1024 pulses per revolution is attached to the motor shaft; the encoder signals are multiplied by four and processed by a FPGA program.

Predictive torque and flux control for the synchronous reluctance machine

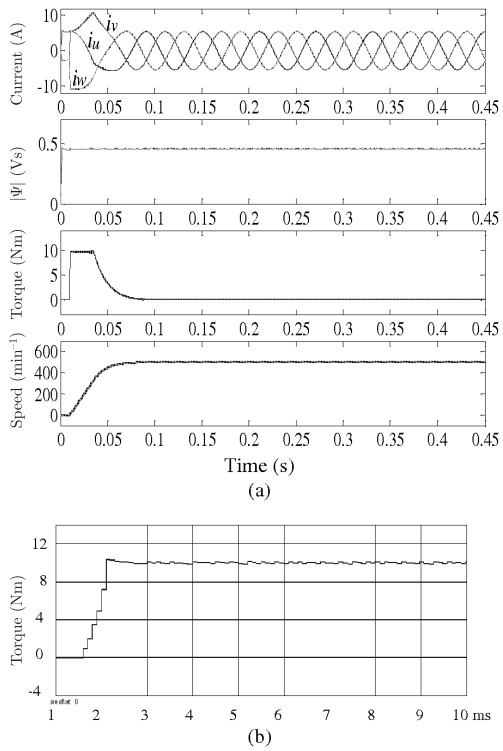


Fig. 9. Simulated run-up of the machine, (a) stator current, flux, torque (calculated) and speed, (b) zoom of the torque signal ($\omega^* = 500 \text{ min}^{-1}$, $M_{\text{Max}} = 10 \text{ Nm}$ $\Psi^* = 0.45 \text{ Vs}$, and 300 V on U_{dc})

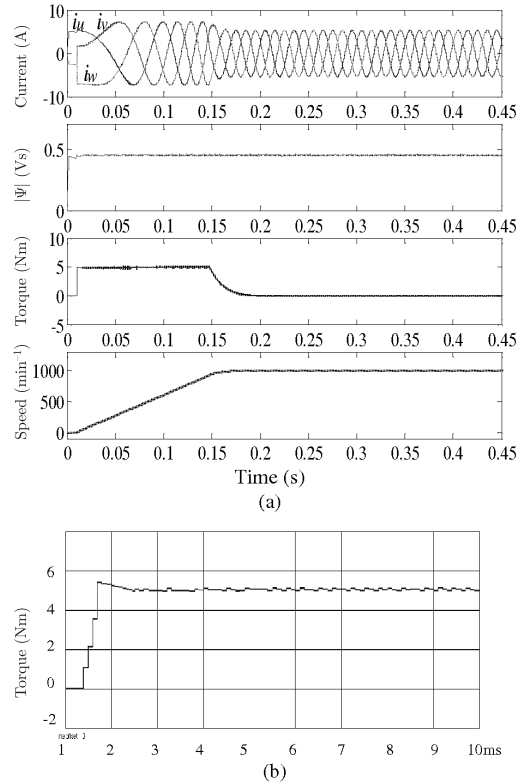


Fig. 11. Simulated run-up of the machine, (a) stator current, flux, torque (calculated) and speed, (b) zoom of the torque signal ($\omega^* = 1000 \text{ min}^{-1}$, $M_{\text{Max}} = 10 \text{ Nm}$ $\Psi^* = 0.45 \text{ Vs}$, and 300 V on U_{dc})

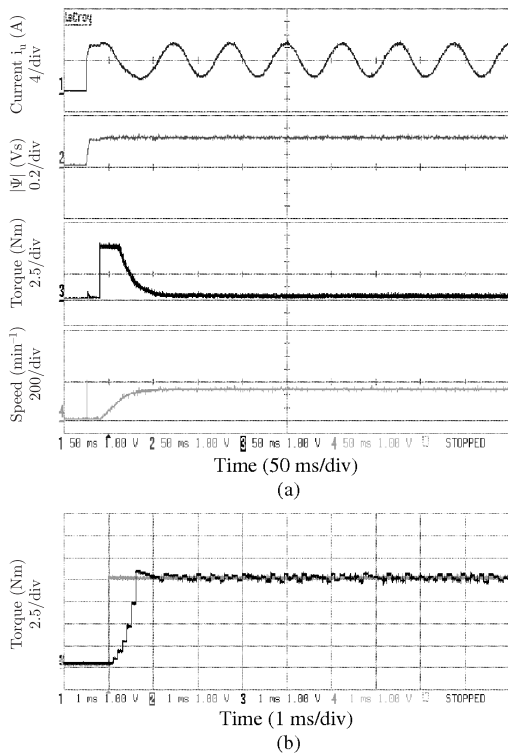


Fig. 10. Experimental run-up of the machine, (a) stator current, flux, torque (calculated) and speed, (b) zoom of the torque signal ($\omega^* = 500 \text{ min}^{-1}$, $M_{\text{Max}} = 10 \text{ Nm}$ $\Psi^* = 0.45 \text{ Vs}$, and 300 V on U_{dc})

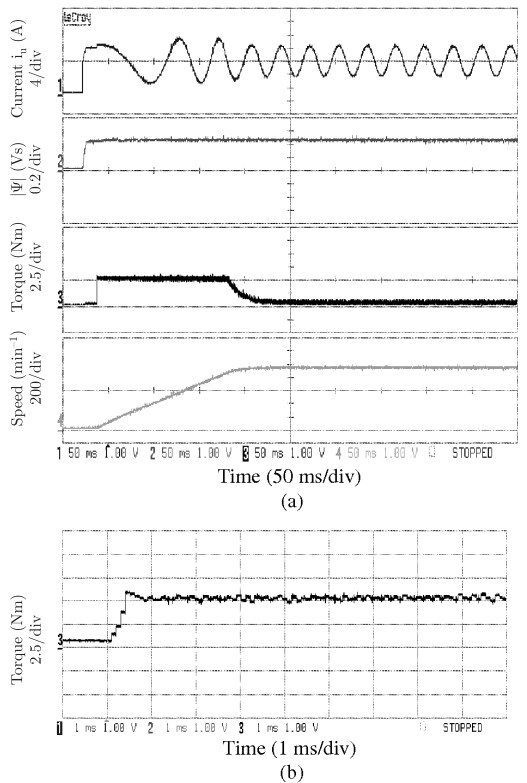


Fig. 12. Experimental run-up of the machine, (a) stator current, flux, torque (calculated) and speed, (b) zoom of the torque signal ($\omega^* = 1000 \text{ min}^{-1}$, $M_{\text{Max}} = 10 \text{ Nm}$ $\Psi^* = 0.45 \text{ Vs}$, and 300 V on U_{dc})

A laptop computer has been used to command the reference values.

During flux build-up mode for start-up the AVSP \underline{u}_1 is selected for the magnetization of the machine.

The parameters of the SyncRel used in this work are listed in the Appendix.

Figure 7 shows comparative results of simulations for the flux during the start-up of the machine under the same conditions. Figure 7(a) shows the trajectory of the flux without prediction algorithm and Fig. 7(b) with the developed scheme. With the predictive strategy the flux follows the command in an optimum way.

Figure 8 shows experimental results of the stator flux trajectory at start-up. The magnitude of the stator flux is slowly established on its reference to prevent excessive current overshoot.

Figure 9 shows the results of the simulation of the run-up of the motor to 500 min⁻¹ using a model that includes the cross saturation. The torque is limited to 10 Nm, the reference value for the flux is 0.45 Vs and the dc-link voltage is 300 V.

At the beginning the selected voltage space phasor is fully turned “on” during the whole sampling time in order to ensure a fast development of the torque. However, due to the limited voltage and the high value of the inductance at low values of the stator currents (see Fig. 4) the reference value of the torque cannot be achieved within one cycle. Thus, the control chooses during several cycles only the active voltage space phasor and skips the zero voltage space phasor until the reference value of the torque is reached (see Fig. 9 (b)).

Figures. 10 (a) and 10 (b) show the results of the experimental behavior of the machine, when the same reference values as in Fig. 9 were applied. In this experimental run-up it is noted that responses are similar with the respective simulated results and the proposed predictive torque control algorithm shows an excellent performance in terms of torque and flux characteristics.

Figure 11 (a) shows the simulated results for a run-up of the machine to 1000 min⁻¹, the torque is limited to a maximum value of 5 Nm, the flux reference is 0.45 Vs and the dc-link voltage is 300 V. In Fig. 11 (b) the torque signal is zoomed and it can be seen that the torque reaches the reference value with a small settling time and exhibits a low ripple. The experimental results corresponding to Figs 11 (a) and 11 (b) are shown in Figs. 12 (a) and 12 (b).

It can be seen that the responses are similar with their respective simulated results, and the proposed predictive torque control algorithm shows again excellent performance in terms of torque and flux characteristics.

It is obvious that a solution can only be found if the necessary voltage is available. Especially at high speeds the desired torque cannot be reached in one step. So at a certain level of the voltage close to the voltage limit, the algorithm requires a special treatment, otherwise an over current may occur [15].

5. Conclusions

A new predictive torque control algorithm for the synchronous reluctance machine that is suitable for digital implementation has been presented, in which the torque ripple is not as high as in digital implementations of a conventional DTC.

Normally, the torque control has the higher priority and the control scheme tries to fulfill the torque demand. Yet in some cases, it is necessary to find a compromise between the demands of the torque and the flux-controller. This problem was resolved with a flux prediction algorithm that selects the optimum voltage space phasor, which brings the flux closest to its reference value.

The cross coupling has a high impact on the dynamic behavior of the drive and it should be taken into consideration, otherwise the prediction is inaccurate and the torque ripple becomes unfavorable.

An appropriate model is also essential for high performance sensorless drive from zero speed, where the rotor angle is estimated exploiting the anisotropic properties of the machine. This will be the next topic of investigation.

Appendix

Data of the machine:

Rated torque	$M_r = 27 \text{ Nm}$
Rated current	$I_r = 14.6 \text{ A}$
Number of poles	$p = 2$
Stator resistance	$R_S = 0.34 \Omega$
Rotor inertia	$J = 7.041 \cdot 10^{-3} \text{ kgm}^2$

REFERENCES

- [1] T. A Lipo, “Synchronous reluctance machines – a viable alternative for ac drives?”, *Electric Machines & Power Systems* 19, 659–671 (1991).
- [2] A. Kiltthau and M. Pacas, “Parameter-measurement and control of the synchronous reluctance machine including cross saturation”, *IEEE/IAS Annual Meeting*, Chicago, USA, on CD (2001).
- [3] A. Kiltthau and M. Pacas, “Appropriate models for the control of the synchronous reluctance machine”, *IEEE/IAS Annual Meeting*, Pittsburgh, USA, on CD (2002).
- [4] A. Kiltthau, *Drehgeberlose Regelung der Synchronen Reluktanzmaschine*; Dissertation, University of Siegen, 2002.
- [5] R. Lagerquist, I. Boldea, and T. Miller. “Sensorless control of the synchronous reluctance motor”, *IEEE Trans. Industrial Applications* 30 (3), 673–682 (1994).
- [6] I. Boldea, Z. X. Fu, and S. A. Nasar, “Torque vector control (TVC) of axially-laminated anisotropic (ALA) reluctance motors”, *Electric Machines & Power Systems* 19, 381–398 (1991).
- [7] I. Boldea, L. Janosi, and F. Blaabjerg, “A modified direct torque control (DTC) of reluctance synchronous motor sensorless drive”, *Electric Machines & Power Systems* 28 (2), 115–128 (2000).
- [8] M. P. Kaźmierkowski, R. Krishnan, and F. Blaabjerg, *Control in Power Electronics*, San Diego: Academic Press, 2002.
- [9] A. Consoli, C. Cavallaro, G. Scarcella, and A. Testa. “Sensorless torque control of SyncRel motor drives”, *IEEE Trans. Power Electronics* 15 (1), 28–35 (2000).
- [10] M. Depenbrock, “Direkte Selbstregelung (DSR) für hochdynamisch Drehfeldantriebe mit Stromrichterspeisung, etz Archiv, Bd. 7 (7), 211–218 (1985).

Predictive torque and flux control for the synchronous reluctance machine

- [11] I. Takahashi and T. Noguchi, "A new quick response and high efficiency control strategy of an induction motor", *IEEE Trans. Industrial Applications* 22 (5), 820–827 (1986).
- [12] E. Flach, R. Hoffmann, and P. Mutschler, "Direct mean torque control of an induction motor", *EPE '97 Trondheim/Norway* 3, 672–677 (1997).
- [13] E. Flach, "Improved algorithm for direct mean torque control of an induction motor", *PCIM 98 Intelligent Motion*, Nuremberg, Germany, 261–267 (1998).
- [14] E. Flach, *Direkte Regelung des Drehmomentmittelwertes einer Induktionsmaschine*, Dissertation, Darmstadt University, 1999.
- [15] J. Faßnacht and P. Mutschler, "Direct mean torque control with improved flux control", *EPE 2003*, Toulouse, France, on CD (2003).
- [16] M. Pacas and J. Weber, "Predictive direct torque control for the PM synchronous machine", *IEEE Trans. Ind. Electron.* 52, 1350–1356 (2005).
- [17] M. Pacas and R. Morales, "A predictive torque control for the synchronous reluctance machine taking into account the magnetic cross saturation", *IECON 05*, Raleigh, USA, on CD (2005).